Can I transform my understanding of **genomics, transcriptomics, and epigenomics** at single cell resolution?

Uncover the full spectrum of cellular diversity and cellular interactions

Unmask true genetic diversity and map clonal evolution in complex disease

Unravel the epigenetic basis of disease and development cell by cell

Get a Multidimensional View of Complex Cellular Systems with Single Cell Solutions from 10x Genomics

Single Cell Transcriptomics

- Gene Expression Profiling
- Gene Expression CRISPR Screening
- Gene Expression & Cell Surface Protein
- Immune Profiling
- Immune Profiling & Cell Surface Protein
- Immune Profiling & Antigen Specificity

Single Cell Genomics

- Copy Number Variation

Single Cell Epigenomics

- Chromatin Accessibility

LEARN MORE AT 10XGENOMICS.COM/YES

10X GENOMICS

![Stem Cells logo]

Barrier Properties and Transcriptome Expression in Human iPSC-Derived Models of the Blood–Brain Barrier

LOUISE DELSING ,[a,b,c] PIERRE DÖNNES,[d] JOSÉ SÁNCHEZ,[e] MARYAM CLAUSEN,[c] DIMITRIOS VOULGARIS,[g] ANNA FALK,[f] ANNA HERLAND,[g,h] GABRIELLA BROLÉN,[c] HENRIK ZETTERBERG,[a,i,j,k] RYAN HICKS,[c] JANE SYNNERGREN[b]

Key Words. Blood–brain barrier • Coculture • hiPSC • In vitro models • Transcriptome • Endothelial cells

[a]Department of Neurochemistry, Institute of Neuroscience and Physiology, The Sahlgrenska Academy at the University of Gothenburg, Gothenburg, Sweden; [b]Systems Biology Research Center, School of Bioscience, University of Skövde, Skövde, Sweden; [c]Discovery Sciences, IMED Biotech Unit, AstraZeneca, Mölndal, Sweden; [d]SciCross AB, Skövde, Sweden; [e]Biostatistics, IMED Biotech Unit, AstraZeneca, Mölndal, Sweden; [f]Department of Neuroscience, Karolinska Institutet, Stockholm, Sweden; [g]Department of Micro and Nanosystems, KTH Royal Institute of Technology, Stockholm, Sweden; [h]Department of Physiology and Pharmacology, Karolinska Institutet, Stockholm, Sweden; [i]Clinical Neurochemistry Laboratory, Sahlgrenska University Hospital, Mölndal, Sweden; [j]Department of Molecular Neuroscience, UCL Institute of Neurology, London, UK; [k]UK Dementia Research Institute at UCL, London, UK

Correspondence: Louise Delsing, M.Sc., University of Skövde, School of Bioscience, Högskolevägen Box 408 541 28 Skövde, Sweden. e-mail: louise.delsing@his.se. Telephone: 46730315638

ABSTRACT

Cell-based models of the blood–brain barrier (BBB) are important for increasing the knowledge of BBB formation, degradation and brain exposure of drug substances. Human models are preferred over animal models because of interspecies differences in BBB structure and function. However, access to human primary BBB tissue is limited and has shown degeneration of BBB functions in vitro. Human induced pluripotent stem cells (iPSCs) can be used to generate relevant cell types to model the BBB with human tissue. We generated a human iPSC-derived model of the BBB that includes endothelial cells in coculture with pericytes, astrocytes and neurons. Evaluation of barrier properties showed that the endothelial cells in our coculture model have high transendothelial electrical resistance, functional efflux and ability to discriminate between CNS permeable and non-permeable substances. Whole genome expression profiling revealed transcriptional changes that occur in coculture, including upregulation of tight junction proteins, such as claudins and neurotransmitter transporters. Pathway analysis implicated changes in the WNT, TNF, and PI3K-Akt pathways upon coculture. Our data suggest that coculture of iPSC-derived endothelial cells promotes barrier formation on a functional and transcriptional level. The information about gene expression changes in coculture can be used to further improve iPSC-derived BBB models through selective pathway manipulation. STEM CELLS 2018; 00:1–12

SIGNIFICANCE STATEMENT

To improve blood-brain barrier (BBB) models and understand BBB function in health and disease there is a need to increase knowledge around molecular mechanisms behind the restricted permeability across the BBB. To our knowledge, this is the first publication describing whole genome expression changes that occur in induced pluripotent stem cell-derived endothelial cells upon co-culture with induced pluripotent stem cell-derived astrocytes, neurons and pericytes. The ability of the endothelial cells to restrict permeability is increased after co-culture, our analysis increases understanding of molecular mechanisms that govern this permeability restriction. Our results can be used to design novel improvement strategies for BBB models.

INTRODUCTION

The blood–brain barrier (BBB) constitutes the interface between the blood and the brain tissue. Its primary function is to maintain the tightly controlled microenvironment of the brain [1]. At the basolateral (brain) face of the endothelial cells (EC), the extracellular basal lamina surrounds the EC and embeds the pericytes. Astrocytic end-feet are in contact with the EC and the basal lamina. This unit of astrocytes, pericytes, basal lamina, and EC is often referred to as the neurovascular unit (NVU) [2, 3]. The EC of the central nervous system (CNS) have specific properties that allow them to restrict permeability between the blood and the brain [3]. The tight cellular interactions between the CNS EC in the BBB act as a physical barrier for pathogens, cells, proteins, and water-soluble agents. Specific transport proteins control the supply of nutrients and the transfer of other small molecules to the brain. A highly active enzyme pool acts as a metabolic barrier within the EC and efflux transport proteins maintain the homeostasis of small gaseous and lipophilic compounds that diffuse across the endothelial apical (blood) membrane [4].

Models of the BBB are important tools in drug development and support the evaluation of the brain-penetrating properties of novel drug molecules. Current models of the BBB range from in vivo animal models to more complex cell models with cocultures of several primary cell types, as well as computer-based in silico models [5–10]. in vivo animal models of BBB permeability, using techniques such as brain perfusion, are currently considered the most accurate. However, these models are time-consuming, expensive and have low-throughput compared with cell models [11]. Primary porcine and bovine cells have high barrier integrity and low permeability [9, 12]. However, primary cells require resource-demanding isolation procedures, have limited availability, and suffer from batch-to-batch variation. Additionally, when the BBB is modeled using animal cells it is important to consider interspecies differences. For example, there are species differences in the expression of BBB transporters, including the important efflux transporter P-glycoprotein (P-gp) [13, 14] and differences between humans and rodents in permeability of P-gp substrates [15].

The availability of primary human brain cells is very limited and samples are typically residual tissue from patient biopsies or postmortem brains. While the use of immortalized cell lines from human and animal origin can circumvent issues with reproducibility and batch-to-batch variation, many of the human brain EC lines fail to form tight cellular interactions [9, 16, 17]. In addition, isolated primary brain EC rapidly lose their BBB properties when cultured in vitro [18, 19]. Therefore, it is plausible that the BBB properties are not intrinsic to the human brain EC but rather depend on the specific microenvironment that all components of the NVU create together. Several coculture models have been described that demonstrate improved barrier properties compared to EC alone [5, 6, 20–22]. The molecular mechanisms underpinning how coculturing cells affect the barrier properties of EC are poorly characterized but signaling through the WNT, NOTCH, and Sonic Hedgehog pathways have been implicated [17, 23, 24].

Recently, models using human induced pluripotent stem cell (iPSC)-derived cells have gained large interest and several coculture models have been reported [25–28]. These have several advantages including their human origin, availability and high reproducibility. Previous models have shown, that iPSC-derived EC cocultured with neural cell types can serve as a predictive model system for BBB permeability [27, 28].

In the present study, we compared of two different protocols to derive EC and used these iPSC-derived EC to establish in vitro coculture models of the BBB. Whole genome expression profiling was performed to elucidate transcription changes behind the BBB specification of EC initiated during coculture.

METHODS

Cell Culture

Two iPSC lines were used to derive EC, SFC-SB-AD2–01, and r-iPSC 1j. r-iPSC 1j was generated from human fibroblasts (ATCC) (male, newborn) using mRNA reprogramming [29], SFC-SB-AD2–01 (Innovative Medicines Initiative Joint Undertaking StemBancc) was generated from fibroblasts (male, 51 years old) using Sendai virus reprogramming. SFC-SB-AD2–01 and r-iPSC 1j were maintained in DEF-CS culture system (Takara Bio). iPSC-derived astrocytes and neurons (both Cellular Dynamics)

were cultured according to the vendor's instructions. Blood–brain barrier hCMEC/D3 cell line (EMD Millipore) was cultured according to the vendor's instructions. Primary human brain microvascular endothelial cells (hBMEC) (ACBRI 376, Cell Systems) were cultured in complete classic medium with serum and CultureBoost (Cell Systems).

Differentiation to EC and Pericytes

Differentiation to EC was performed according to two previously published protocols. Protocol 1 uses a shorter differentiation, relying predominantly on spontaneous differentiation capacity [22, 30]. Protocol 2 applies an approach using directing mitogens and immunomagnetic separation for purification [31] and generates both EC and pericytes. Hereafter, EC derived using Protocol 1 are referred to as iPS-EC1 and EC derived with Protocol 2 are referred to as iPS-EC2.

Protocol 1

iPSCs were seeded at 10,000 cells/cm^2 in DEF-CS 2 days before differentiation start. Once the cells had reached 30,000 cells/cm^2 differentiation was initiated by changing to unconditioned media [UM, DMEM/F12 + glutamax, 20% KOSR, ×1 Nonessential amino acids and 0.1 mM beta-mercaptoethanol (Gibco)]. Cultures were given fresh UM daily, for 6 days. On Day 6, UM was changed to endothelial cell media 1 [ECM1, ES-SFM (Life Technologies), 1% platelet poor serum (Alfa Aesar), 10 μM Retinoic acid (Sigma Aldrich), and 20 ng/ml bFGF (Peprotech)]. On Day 8, cells were passaged at 1,000,0000 cells/cm^2 on to collagen IV (400 μg/ml, EMD Millipore)/fibronectin (100 μg/ml Sigma Aldrich)-coated 24 well 0.4 μm pore polyester membrane Transwell inserts (Corning) or at 250,000 cells/cm^2 on to collagen/fibronectin-coated CellBind Surface 96 well plates (Corning). At day nine media was changed to ECM1 without bFGF and Retinoic acid.

Protocol 2

iPSCs were seeded at 70,000 cells/cm^2 in DEF-CS, the day after differentiation was initiated by changing the media to Mesoderm induction media [APEL2 (Stem Cell Technologies) with 5% PFHM-II Protein-Free Hybridoma Medium (Gibco), 25 ng/ml Activin A (Peprotech), 30 ng/ml BMP4 (R&D Systems), 50 ng/ml VEGF (Sigma Aldrich), and 1.5 μM Chir99021 (Tocris)], media was changed daily for 3 days. On Day 3, media was changed to Vascular specification media [APEL2 (Stem Cell Technologies) with 5% PFHM-II Protein-Free Hybridoma Medium (Gibco), 50 ng/ml VEGF (Sigma Aldrich), and 10 μM SB431542 (Tocris)], media was changed every other day until Day 11, when immunomagnetic separation was performed. Cells were separated using Dynabeads CD31 Endothelial cell (Invitrogen) according to the manufacturer's instruction. After sorting, CD31 positive cells were further expanded by seeding at 10,000 cells/cm^2 on gelatin-coated surfaces (0.01%) in endothelial cell media 2 [ECM2, EC-SFM (Life Technologies) with 1% platelet poor serum (Alfa Aesar), 30 ng/μl VEGF (Sigma Aldrich), and 20 ng/ml bFGF (Peprotech)]. When confluent, cells were passaged at 1,000,000 cells/cm^2 on to collagen (400 μg/ml)/fibronectin (100 μg/ml) covered 24 well 0.4 μm pore polyester membrane transwell inserts (Corning) or at 250,000 cells/cm^2 in collagen/fibronectin-coated CellBind Surface 96 well plates (Corning). CD31 negative cells were expanded on 0.01% gelatin (Sigma Aldrich) coated surfaces in EGM2 media (Lonza) and then further differentiated to

pericytes by culturing in pericyte differentiation media [DMEM/F12 (Gibco) with 10% FBS (Stem Cell Technologies), 2 ng/ml TGF-β3 (Sigma Aldrich), and 4 ng/μl PDGF-bb (R&D Systems)] for 3 days. Pericytes were then maintained in DMEM/F12 (Gibco) with 10% FBS (Stem Cell Technologies).

Coculture Setup

Astrocytes were seeded at 40,000 cells/cm^2 on matrigel (Corning) coated 24-well plates (Corning), 2 days before the start of coculture. The day before the start of coculture, pericytes were seeded at 50,000 cells/cm^2 on to the lower side of collagen/fibronectin-coated transwell inserts. Neurons were seeded at 25,000 cells/cm^2 on top of the astrocytes. EC were seeded at 1,000,000 cells/cm^2 on Transwell membranes coated with collagen/fibronectin as described above, and allowed to attach for at least 6 hours. Coculture was initiated by changing the media in the astrocyte-neuron coculture to 1 ml endothelial media, and inserting the Transwell membrane with pericytes on the bottom and EC on top. Analyses were performed at 3, 5, and 8 days after coculture initiation. A schematic of the coculture setup is shown in Figure 1C.

Immunocytochemistry

Cells were seeded at 250,000 cells/cm^2 in CellBind Surface 96-well plates (Corning) as described in the cell culture section, at least 24 hours before fixation. Cells were washed with 100 μl PBS and subsequently incubated with 50 μl methanol (Sigma Aldrich) at −20°C or 4% PFA (Ninolab) at RT, for 20 minutes. The cells were then washed three times with 100 μl PBS and incubated at RT for 1 hour with 100 μl blocking and permeabilizing buffer containing 10% FBS (Life Technologies) and 0.1% Triton-X (Sigma Aldrich) in PBS. Primary antibodies were diluted in antibody buffer (PBS containing 5% FBS and 0.1% Triton-X) according to Supporting Information S1. The 50 μl primary antibody solution was incubated with the cells at RT for 2 hours,

followed by three washes with 100 μl PBS. The secondary antibodies used were Alexa Fluor 488-conjugated anti-mouse (Life Technologies) and Alexa Fluor 594-conjugated anti-rabbit (Life Technologies) diluted 1,000× in antibody buffer. The 50 μl secondary antibody solution was incubated with the cells for 40 minutes at RT followed by 10 minutes incubation with 50 μl of 4′,6-diamidino-2-phenylindole (DAPI) solution. DAPI solution contained 1 μg/ml DAPI (Invitrogen) in antibody buffer. Finally, cells were washed with 100 μl PBS 4 times. Image acquisition was performed with an ImageXpress Micro XLS Widefield High-Content Analysis System (Molecular Devices).

Transendothelial Electrical Resistance Measurements

Transendothelial electrical resistance (TEER) measurements were carried out using an EVOM [2] Epithelial Voltohmmeter (World Precision Instruments). The resistance value was calculated using the equation below. Empty filters coated with collagen/fibronectin were used as blanks. All TEER measurements were performed in triplicates.

$$\left(\text{TEER}\,\Omega \times \text{cm}^2\right) = \left(\text{TEER(EC)} - \text{TEER(blank)}\right) \times \text{Area of culture}$$

Sodium Fluorescein Permeability

Cells were washed with HBSS (Life Technologies) before addition of Sodium Fluorescein (NaF, Sigma Aldrich) at 1 μM in HBSS to the apical chamber and HBSS to the basolateral chamber. Cells were incubated on a rotating platform for 60 minutes at 37°C. NaF concentration in the basolateral compartment was calculated after measuring fluorescence on a plate reader (485 nm excitation and 535 nm emission).

Efflux Transporter Activity

Efflux transporter activity was assessed by the permeability of P-gp substrate rhodamine 123 (Sigma Aldrich) or BCRP
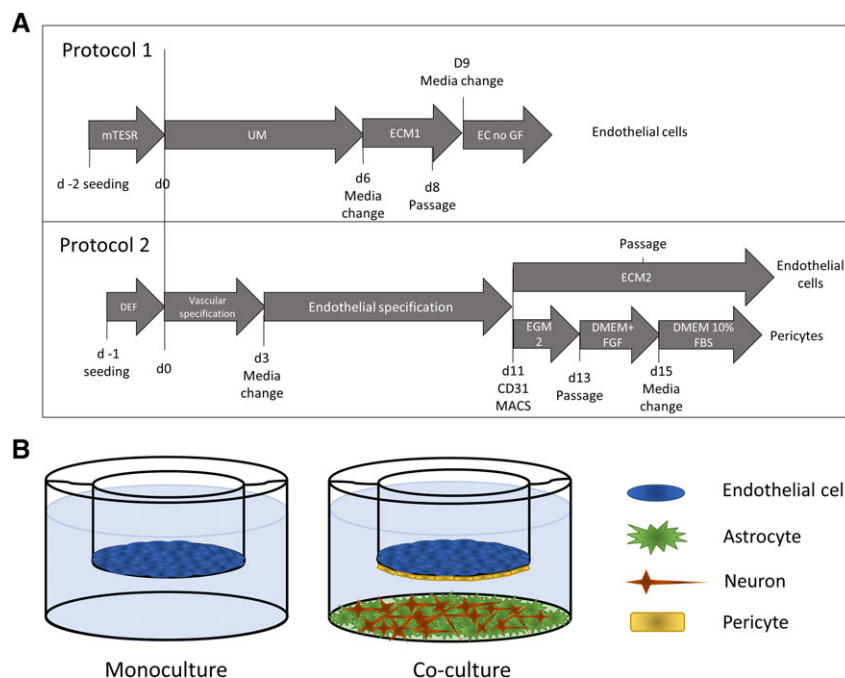

Figure 1. Overview of differentiation protocols for conversion of iPSCs to EC and the coculture setup. **(A):** Schematic overview of protocols used to derive EC from iPSCs. **(B):** Schematic overview of the BBB model setup. Monocultures (right) are compared to cocultures (left).

substrate dantrolene (AstraZeneca) with and without the addition of the P-gp inhibitor verapamil (AstraZeneca) at 50 µM or the BCRP inhibitor Ko 143 (Tocris) at 5 µM. iPSC-derived EC in monoculture or coculture were preincubated with or without inhibitor in HBSS (Life Technologies) for 30 min. The cells were then incubated with 10 µM rhodamine 123 or 1 µM dantrolene, with or without inhibitor, for 1 hour. All incubations were performed at 37°C on a rotating platform. For rhodamine permeability experiments fluorescence was measured on a plate reader (485 nm excitation and 535 nm emission) and reported as the normalized permeability. Dantrolene levels were measured by LC–MS and reported as normalized permeability.

Permeability Experiments

The apparent permeability (P_{app}) of six substances across EC in monoculture and coculture were investigated on a rotating platform at 37°C after 3 days of coculture. Atenolol, erythromycin, verapamil, dantrolene, phenytoin (AstraZeneca), and propranolol (Merck) were diluted to a final concentration of 1 µM in transport buffer [HBSS (Gibco) with 25 mM HEPES (Gibco) pH 7.4)]. Cells were washed once before addition of the substances with either the apical (200 µl) or basolateral side (800 µl), substance-free buffer was added to the other side. Samples were taken at 10, 30, and 60 minutes. The concentration of each substance in the samples was determined by LC–MS, and apparent permeability and efflux ratio were calculated as previously described [32]. All permeability studies were performed in triplicate and were preceded and followed by TEER measurements to ascertain retained EC monolayer integrity. The substances were selected based on their chemical properties, see Supporting Information S8.

mRNA Expression Analysis

A minimum of 200,000 EC were collected and RNA was purified using the RNeasy Mini Kit (Qiagen) with DNase treatment according to the manufacturer's instructions. RNA was reverse transcribed using the High-Capacity cDNA Reverse Transcription kit (Applied Biosystems). cDNA amounts were detected using TaqMan gene expression assays (Applied Biosystems) (Supporting Information S2) on a 7900HT Sequence Detection System (Applied Biosystems). Three technical replicates of three independently differentiated biological samples were used at each data point. Expression data were analyzed and related to the level of GAPDH using the dCt method [33].

mRNA Library Construction and Sequencing

RNA was isolated as described above. The RNA quality was assessed by a Fragment Analyzer (Advanced Analytical Technologies). One microgram of total RNA was used for each library. Illumina TrueSeq Stranded mRNA LT Sample Prep Kit (Illumina) was used to construct poly(A) selected paired-end sequencing libraries according to TrueSeq Stranded mRNA Sample Preparation Guide (Illumina). All libraries were quantified with the Fragment Analyzer (Advanced Analytical Technologies), pooled and quantified with Qubit Fluorometer (Invitrogen) and sequenced using Illumina NextSeq 500 sequencer (Illumina). Three biological replicates were sequenced per condition.

RNAseq Processing and Analysis

RNAseq data were processed using Blue Collar Bioinformatics (bcbio-nextgen). The sequencing reads were aligned to the human genome (hg38) via Hisat2, and read counts were summarized and annotated using Sailfish and Htseq-count. Differentially expressed genes were identified using the DESeq2 algorithm using the Wald test with false discovery rate (FDR) adjustment for multiple comparisons [34]. A combined criteria of fold change (FC) > 1.5 and $p < .01$, was applied to compare the different conditions. The GO enrichment analysis was based on the PANTHER classification system [35]. We further investigated junction associated proteins [36, 37], ABC transporters [38] and SLC transporters [39] commonly associated with the BBB. To search for differentially expressed pathways between the monoculture and coculture of iPS-EC1, the DAVID tools [40] were used to search the KEGG database [41].

Statistical Analysis

Student's t test with two-tailed distribution, assuming equal standard deviation, was used for statistical analysis if not otherwise specified.

RESULTS

Protocols and Differentiation

Two different protocols for EC generation from iPSCs were evaluated (Fig. 1A). Brightfield images display the characteristic morphology of cells during differentiation (Supporting Information S3). Cultures were setup in Transwells with EC seeded on the top of the membrane (Fig. 1B). In cocultures, pericytes were seeded on the bottom of the membrane with astrocytes and neurons on the bottom of the plate. The two protocols were tested with two iPSC lines; r-iPSC 1j (Fig. 2–3), SFC-SB-AD2–01 (Supporting Information S4) with similar results.

Characterization of EC-Derived with Either Protocol 1 (iPS-EC1) or Protocol 2 (iPS-EC2)

We characterized the iPS-EC1 and iPS-EC2 cells by immunostaining for EC markers, tight junction-associated protein zonula occludens-1 (Zo-1), tight junction protein claudin 5, cellular adhesion protein CD31, glucose transporter Glut-1, von Willebrand factor (vWF), tight junction protein occludin, adherence junction protein VE-cadherin, and caveolae-related protein caveolin1. The iPS-EC1 (Fig. 2A) and iPS-EC2 (Fig. 2B) show staining for Zo-1, claudin 5, CD31, Glut1, vWF, and caveolin1. CD31 and VE-cadherin staining appear more distinct in iPS-EC2 than in iPS-EC1. iPS-EC1 show uniform Glut-1 and occludin staining while iPS-EC2 only show Glut-1 staining for a subset of cells and no occludin staining. iPS-EC2 shows stronger staining for caveolin1 and vWF compared to iPS-EC1. The BBB hCMEC/D3 cell line and hBMEC were included as controls (Fig. 2C and Supporting Information S5). Both show staining for Zo-1, claudin 5 (partial for hCMEC/D3), CD31 (partial for hCMEC/D3), and vWF. hCMEC/D3 show more distinct cell junction staining for VE-cadherin. Glut1 staining is lower in hBMEC than in hCMEC/D3. Only iPS-EC1 shows distinct occludin staining.

Characterization of Astrocytes, Pericytes, and Neurons

In the BBB model, EC were cocultured with astrocytes, pericytes, and neurons. Immunocytochemistry of these cell types are shown in Supporting Information S6. Pericytes derived from iPSCs using Protocol 2, expressed caldesmon, partial-smooth muscle actin alpha (SMA), and smooth muscle-specific protein 22 (SM22). Astrocytes expressed the astrocyte-specific
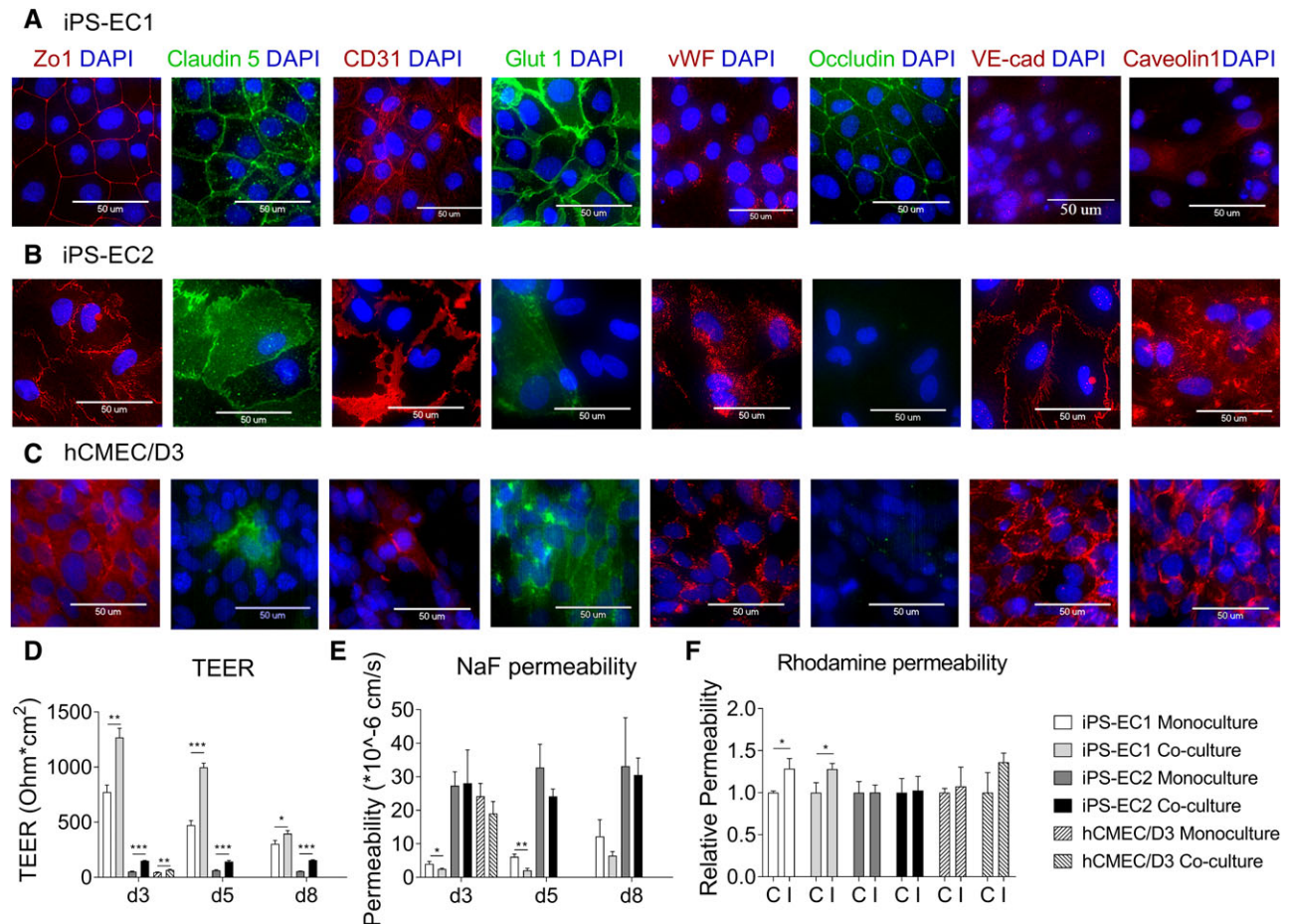
Figure 2. Characterization of induced pluripotent stem cell (iPSC)-derived EC with protocol 1 (iPS-EC1) and protocol 2 (iPS-EC2). **(A–C)**: Representative immunocytochemistry staining images of iPS-EC1 **(A)**, iPS-EC2 **(B)**, and hCMEC/D3 **(C)**. Cells were stained for zonula occludens-1 (ZO-1), tight junction proteins claudin 5, cellular adhesion protein CD31, glucose transporter Glut1, von Willebrand factor (vWF), adherence junction proteins occludin, and VE-cadherin (VE-cad), and caveolin1. DAPI (in blue) is staining the nuclei. Scale bar 50 μm. **(D)**: Cell layer tightness as measured by transendothelial electrical resistance (TEER) after 3, 5 and 8 days in monoculture or coculture. Data shown as mean $\pm$ SD of at least three individual experiments, significance in a Student's t test is indicated by *($p < .05$), **($p < .01$), and ***($p < .001$). **(E)**: Permeability of sodium fluorescein at 3, 5, and 8 days of monoculture and coculture. **(F)**: P-glycoprotein efflux activity measured by rhodamine 123 permeability in the absence [C] or presence of P-glycoprotein (P-gp) inhibitor verapamil [I]. Data shown as mean normalized permeability of three individual experiments $\pm$ SD, significance in Student's t test is indicated by *($p < .05$).

intermediate filament glial fibrillary acid protein (GFAP) and S100B. Neurons expressed the neuron-specific tubulin Tuj1 and were mostly negative for the neural progenitor marker nestin.

Comparison of Barrier Properties of iPS-EC1 and iPS-EC2 in Monoculture and Coculture

Coculture of the EC with other cell types of the NVU has previously been shown to influence their barrier properties [5, 6, 20–22]. We investigated the effect of coculturing with astrocytes, pericytes, and neurons in terms of TEER, Sodium Fluorescein (NaF) permeability and P-gp efflux activity. Efflux activity was assayed by rhodamine 123-permeability in the absence [C] or presence of the P-gp inhibitor verapamil [I]. Cell layer tightness, as measured by TEER (Fig. 2D), was clearly higher for iPSC-EC1 in both the monoculture and the coculture compared to iPS-EC2. TEER was significantly increased in the coculture compared to the monoculture for iPS-EC1 (Day 3, 1,267 $\pm$ 68 and 773 $\pm$ 52 Ohm $\times$ cm^2, respectively, $p < .001$), iPS-EC2 (Day 3, 150 $\pm$ 3 and 52 $\pm$ 3 Ohm $\times$ cm^2, respectively, $p < .001$) and hCMEC/D3 (Day 3, 67 $\pm$ 5 and 45 $\pm$ 2 Ohm $\times$ cm^2, respectively, $p < .01$) (Fig. 2D). In iPS-EC1, the

TEER decreased between Days 3 and 8 in both monoculture and coculture (TEER; monoculture $p < .001$, coculture $p < .001$). TEER was unchanged over the investigated time period for iPS-EC2. Passive permeability as measured by NaF permeability (Fig. 2E) was more than 6-fold higher in iPS-EC2 and hCMEC/D3 compared to iPS-EC1, both in monoculture and coculture. NaF permeability was significantly lower in the coculture compared to the monoculture for iPS-EC1. In iPS-EC1, NaF permeability increased significantly between days 3 and 8 in both monoculture and coculture (monoculture $p < .05$, coculture $p < .01$). Rhodamine 123 permeability increased 28% after treatment with P-gp inhibitor in iPS-EC1 ($p < .05$), but was not changed for iPSC-EC2 and hCMEC (Fig. 2F).

The relative mRNA levels of BCRP, P-gp, Glut1, CD31, Zo-1, VE-Cadherin, Caveolin1, Claudin 5, Occludin, and vWF display differences between the protocols (Fig. 3A–J). iPS-EC1 and iPS-EC2 show similar expression for P-gp, Zo1, and Glut1. However, iPS-EC2 show higher expression of CD31, VE-cadherin, caveolin1, claudin 5 and vWF, compared to iPS-EC1. iPS-EC1 shows higher expression for BCRP compared to iPS-EC2. Occludin mRNA levels are similar between iPS-EC1 and iPS-EC2 in monoculture but
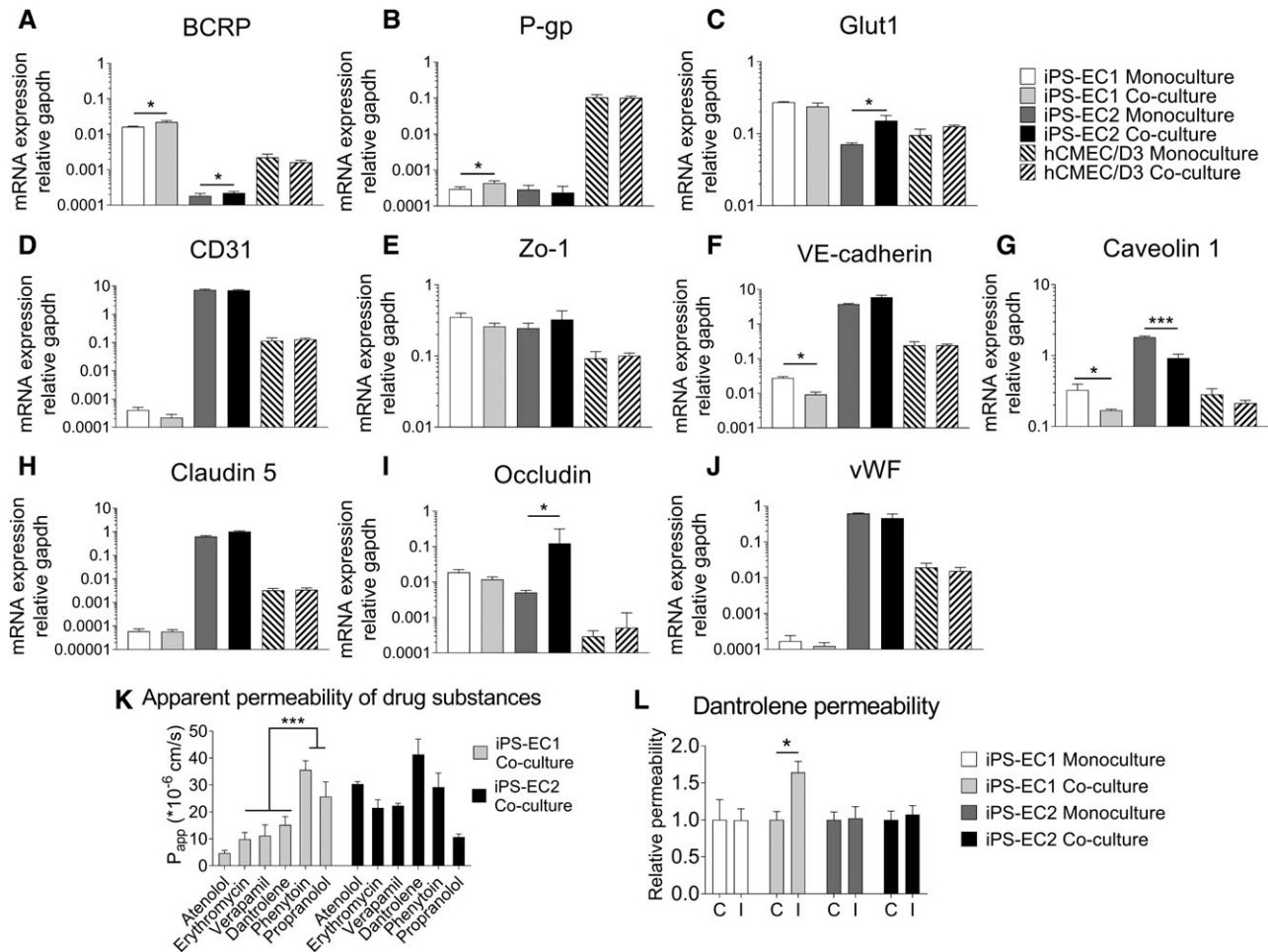
Figure 3. Comparison of the barrier properties of iPS-EC1 and iPS-EC2 in monoculture and cocultures after 3 days of monoculture and coculture. (**A–J**): Relative mRNA expression of transporters BCRP, P-gp, Glut-1, junction associated proteins CD31, ZO-1, VE-cadherin, claudin 5, occludin, and vWF. Data shown as mean $\pm$ SD of individual experiments. The Y-axis is in logarithmic scale. Significance in a Student's t test is indicated by *($p < .05$), **($p < .01$), and ***($p < .001$). White bar represents iPS-EC1 in monoculture, light gray bar represents iPS-EC1 in coculture with astrocytes, pericytes, and neurons, dark gray bar represents iPS-EC2 in monoculture, black bar represents iPS-EC2 in coculture with astrocytes, pericytes, and neurons. Left leaning striped bar represents hCMEC/D3 in monoculture and right leaning striped bar represents hCMEC/D3 in co-culture. (**K**): The apparent permeability of six substances, ordered in rising predicted permeability, across EC iPS-EC1 and iPS-EC2 in coculture with astrocytes, pericytes, and neurons. Apparent permeability was measured in the apical to basolateral direction. Data is presented as mean $\pm$ SD, statistically significant differences between CNS permeable and non-CNS permeable substances in a student's t test is indicated with ***($p < .001$). (**L**): BCRP efflux activity measured by dantrolene permeability in the absence [C] or presence of BCRP inhibitor Ko143 [I]. Data shown as mean normalized permeability of three individual experiments $\pm$ SD, significance in Student's t test is indicated by *($p < .05$).

higher for iPS-EC2 in coculture. The hCMEC/D3 line, iPS-EC1, and iPS-EC2 have similar expression levels for Zo-1 and Glut-1. Expression levels of CD31, claudin 5, VE-cadherin, and vWF are lower in hCMEC/D3 than iPS-EC2 but higher in hCMEC than iPS-EC1. iPS-EC1 has higher expression of BCRP than hCMEC/D3 and hCMEC/D3 have higher expression of P-gp than both iPS-EC1 and iPS-EC2. iPS-EC2 has higher expression of caveolin1 than both iPS-EC1 and hCMEC/D3. Notably, the mRNA expression of BCRP increased in both iPS-EC after coculture ($p < .05$). The expression of P-gp was increased in iPS-EC1 after coculture ($p < .05$) and Glut-1 and occludin expression was increased in iPS-EC2 after coculture ($p < .05$). Caveolin1 mRNA levels were decreased after coculture in both iPS-EC1 and iPS-EC2. mRNA levels at days 3, 5, and 8 of monoculture or coculture reveal changes over time (Supporting Information S7), with levels of some mRNA increasing and some decreasing. However, no general benefit of longer culture time than 3 days could be

distinguished. For iPS-EC1 the maximum tightness in terms of TEER and NaF permeability is at day 3, these measurements did not change over the investigated time period for iPS-EC2. Hence, the permeability and transcriptome analysis were investigated at day 3 of coculture. Taken together, the mRNA levels of P-gp and efflux activity data suggest that iPS-EC1 cells have functional P-gp efflux while iPS-EC2 cells do not.

Permeability of Drug Substances

To investigate transport properties and model these, the permeability of six drug substances was analyzed. The apparent permeability in the apical to basolateral direction was determined for cocultures and monocultures (Fig. 3K and Table 1). The permeability across iPS-EC1 in the coculture was lowest for atenolol followed by erythromycin, verapamil, dantrolene, propranolol, and phenytoin. Substance permeability data across iPS-EC1 in coculture distinguished the substances considered CNS-

Table 1. Apparent permeability of drug substances

		Atenolol	Erythromycin	Verapamil	Dantrolene	Phenytoin	Propanolol
Protocol 1	iPS-EC1 monoculture	10.5 ± 3.1	11.6 ± 3.0	12.5 ± 0.9	22.1 ± 2.3	25.7 ± 1.6	25.1 ± 4.9
	iPS-EC1 coculture	4.7 ± 1.0*	9.9 ± 2.5	11.2 ± 4.0	15.2 ± 3.1	35.6 ± 3.4	22.6 ± 5.5
Protocol 2	iPS-EC2 monoculture	30.4 ± 0.9	21.5 ± 3.0	22.3 ± 0.9	41.3 ± 5.8	29.2 ± 5.2	31.8 ± 3.5
	iPS-EC2 coculture	34.6 ± 8.1	31.8 ± 6.2*	18.3 ± 2.8	45.6 ± 3.7	29.4 ± 10.9	10.7 ± 1.2*

Apparent permeability in apical to basolateral direction across endothelial cells derived with Protocol 1 (iPS-EC1) or Protocol 2 (iPS-EC2) in monoculture or coculture with astrocytes, pericytes, and neurons. Data presented as mean ± SD ($\times 10^{-6}$ cm/s) of three biological replicates.
*Indicates significant difference compared to monoculture ($p < .05$).

permeable from the CNS-nonpermeable ($p < .001$), see Supporting Information S8. The least permeable substance, atenolol, had a significantly lower permeability in the iPS-EC1 coculture compared to the monoculture ($p < .05$). The permeability across iPSC-EC2 in coculture was lowest for verapamil followed by propranolol, phenytoin, erythromycin, atenolol, and dantrolene. The permeability across iPS-EC2 was similar for CNS-permeable and CNS-nonpermeable substances. Propranolol had lower permeability and erythromycin had higher permeability in iPS-EC2 coculture compared to monoculture ($p < .05$).

Efflux Ratio of Drug Substances

The efflux ratio is the ratio between the transport in the apical to basolateral direction and the transport in the basolateral to apical direction. It can be used to evaluate if substances are effluxed by specific transporters. As shown in Table 2, the efflux transporter substrates erythromycin, verapamil, and dantrolene were effluxed to some extent in the iPS-EC1, but not in the iPS-EC2. Higher efflux ratios in the coculture compared to the monoculture were most notable for dantrolene in iPS-EC1, with an efflux ratio of 2.7 in the monoculture and 6.1 in the coculture. However, none of the changes in efflux ratio between monoculture and coculture were found significant. To verify BCRP efflux activity, the permeability of BCRP substrate dantrolene was investigated in the presence [I] and absence [C] of BCRP inhibitor Ko143 (Fig. 3(L)). Dantrolene permeability was increased by 64% in the presence of BCRP inhibitor in iPS-EC1 coculture, no change was detected in iPS-EC1 monoculture or iPS-EC2. In summary, iPS-EC1 in coculture has efflux activity for both P-gp and BCRP substrates.

Transcriptomics Analysis

To characterize molecular mechanisms behind the improved barrier properties of EC in coculture, whole genome expression analysis was performed. iPS-EC1 showed a notably higher number of differentially expressed genes (DEGs) between monoculture and coculture at the given cutoff levels (Fig. 4A). Genes associated with either junction formation or BBB transport were evaluated and displayed as heat maps of normalized counts in monoculture and coculture (Fig. 4C and 4D). Comparing the expression of junction associated genes between the protocols showed that iPS-EC2 had high expression of CLDN5, ICAM1,

ICAM2, PECAM1 (CD31), CDH5 (VE-cadherin), JAM3, and ESAM1, while iPS-EC1 had high expression of CLDN4, CLDN6, and CLDN7. Both iPS-EC 1 and iPSEC2 had high expression of Zo-1 mRNA (TJP1). Among the genes in the heat maps, four junction-associated genes and three transporter genes showed $\log_2$ FC > 1.5 between monoculture and coculture for both protocols (Fig. 4B). The expression of TJP3 increased for both protocols, while CLDN8, CLDN19, and VCAM only increased for iPS-EC1, and CLDN6 only increased for iPS-EC2. The neurotransmitter transporter SLC6A15 increased significantly between monoculture and coculture for both iPS-EC1 and iPS-EC2. iPS-EC1 also showed increased expression of ABCB1 (P-gp) and neurotransmitter transporter SLC6A13 in the coculture compared to the monoculture. GO enrichment analysis was performed to further elucidate the impact of coculture on both protocols. Table 3 shows enriched GO-CC terms among the DEGs between the monoculture and coculture of iPS-EC1 (adjusted p value <.05) that are of high relevance to BBB processes. iPS-EC2 showed fewer enriched GO-CC terms, however all terms identified for iPS-EC2 were also identified for iPS-EC1. Differentially expressed KEGG pathways between the monoculture and coculture of iPS-EC1 were identified. These include the ECM receptor interaction ($p = 1.23 \times 10^{-12}$), cell adhesion molecules ($p = 6.38 \times 10^{-5}$), focal adhesion ($p = 1.08 \times 10^{-8}$), neuroactive ligand-receptor interaction ($p = 3.79 \times 10^{-4}$), the WNT signaling pathway ($p = 4.38 \times 10^{-3}$), the TNF signaling pathway ($p = 6.65 \times 10^{-6}$), and the PI3K-Akt signaling pathway ($p = 1.53 \times 10^{-7}$).

DISCUSSION

To understand how different protocols for deriving EC from iPSCs affect the ability to create an in vitro BBB model, we compared two differentiation protocols and analyzed barrier properties in coculture BBB models. The whole genome expression changes between EC in monoculture and coculture were investigated. In terms of functionally restricting permeability iPSC-EC1 in coculture showed highest performance with high TEER, low NaF permeability, and functional efflux, comparable to other models using similar protocols to derive EC [22, 27]. However, the measured TEER values are lower than some of the

Table 2. Efflux ratio of drug substances

		Atenolol	Erythromycin	Verapamil	Dantrolene	Phenytoin	Propranolol
Protocol 1	iPS-EC1 monoculture	1.18 ± 0.7	2.10 ± 1.1	0.93 ± 0.7	2.27 ± 0.7	1.62 ± 0.2	0.73 ± 0.2
	iPS-EC1 coculture	0.70 ± 0.3	2.16 ± 0.1	1.88 ± 0.6	6.57 ± 3.0	1.13 ± 0.2	0.67 ± 0.1
Protocol 2	iPS-EC2 monoculture	0.71 ± 0.2	0.94 ± 0.2	0.97 ± 0.1	0.84 ± 0.1	1.65 ± 0.3	0.55 ± 0.2
	iPS-EC2 coculture	0.61 ± 0.3	0.97 ± 0.0	0.67 ± 0.2	0.91 ± 0.2	1.61 ± 0.4	0.52 ± 0.1

Efflux ratio in endothelial cells derived with Protocol 1 (iPS-EC1) or Protocol 2 (iPS-EC2) in monoculture or coculture with astrocytes, pericytes, and neurons. Data presented as ratio of means ± SD from three biological replicates.
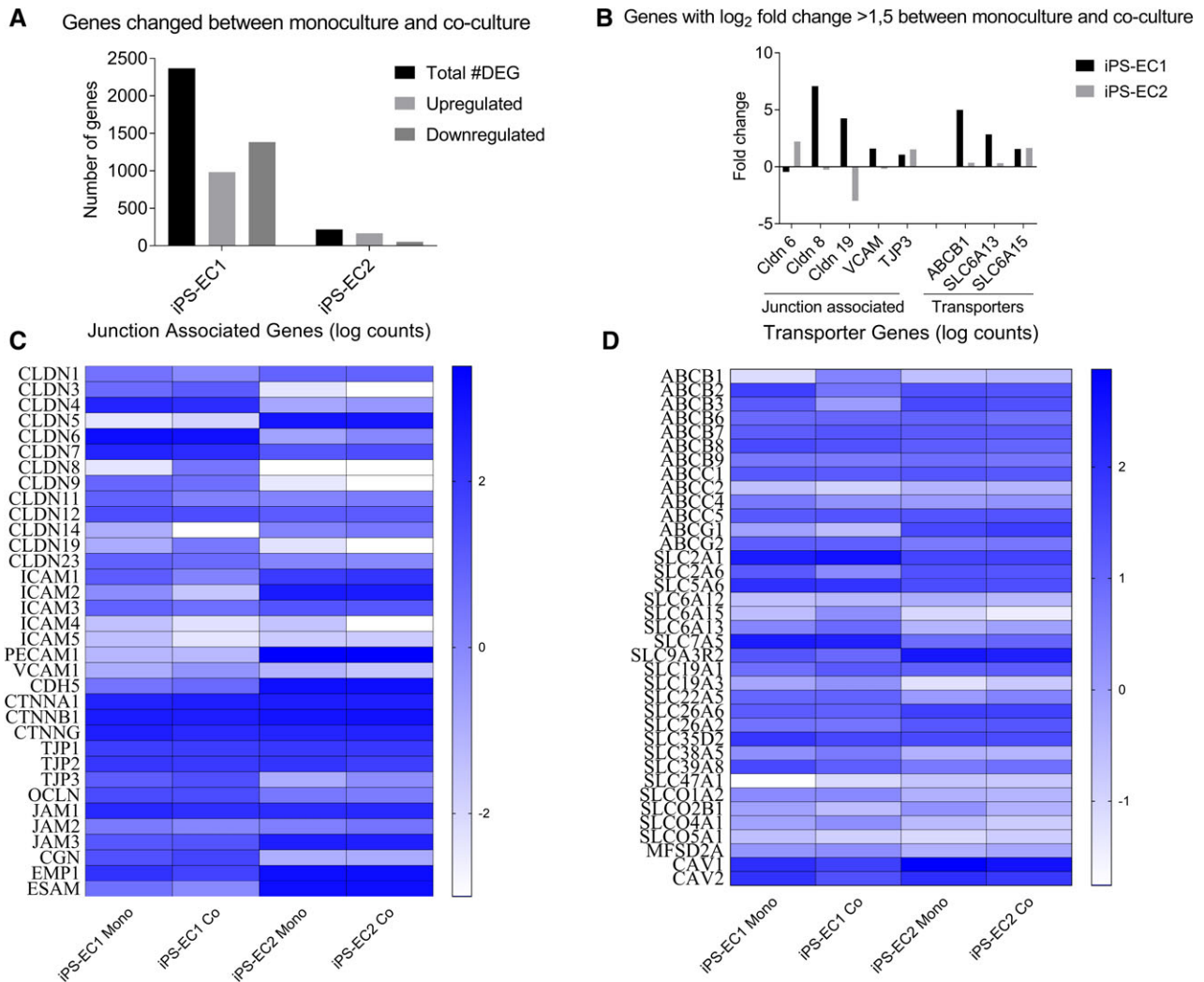
Figure 4. Transcriptome profile comparison between monoculture and cocultures of iPS-EC1 and iPS-EC2. **(A):** Bars show the number of differentially expressed genes between monoculture and coculture. Differentially expressed genes are defined by $\log_2$ fold change (FC) > 1.5 and $p < .01$. **(B):** FC between monoculture and coculture for each protocol of genes identified from heat maps to have a $\log_2$ fold increase > 1.5 and $p < .01$. **(C):** Normalized counts for junction associated genes in monoculture and coculture for each protocol. Data shown as mean of log(counts). **(D):** Normalized counts for transporter genes in monoculture and coculture for each protocol. Data shown as mean of log(counts).

highest reported values for iPSC-derived ECs [25, 26, 28], and previous reports demonstrate that different iPSC lines give different maximum TEER [25, 30]. iPSC-EC2 showed substantially lower TEER and higher NaF than iPSC-EC1, however, in the same range as hCMEC/D3 and other models using similar protocols to derive EC for BBB models [42]. Even though iPS-EC1 shows superior tightness and permeability restriction of the barrier, low expression of proteins and/or mRNA for CD31, VE-cadherin, and vWF, than iPS-EC2 and hCMEC/D3 were observed. These differences highlight an interesting discrepancy between marker expression and functionality in the models. In contrast to our findings, VE-cadherin has been reported to be distinctly detectable with immunocytochemistry in EC derived with Protocol 1 [22, 27, 28]. In our experiments, VE-cadherin staining is much weaker in iPS-EC1 and hBMEC than iPS-EC2 and hCMEC/D3. The mRNA levels for CD31 and VE-cadherin were lower for hCMEC/D3 and iPS-EC1 than for iPS-EC2, demonstrating that VE-cadherin and CD31 are very highly expressed in iPS-EC2. For CD31 this is not surprising as EC in this protocol are selected

based on CD31 expression in magnetic sorting. EC are commonly recognized by their expression of tight junction proteins VE-cadherin [43] and claudin 5 [44], while epithelial cells are recognized by expression of other tight junction proteins such as claudin 7 [45]. In iPS-EC1 mRNA expression of VE-cadherin and claudin 5 are lower while the mRNA expression of claudin 7 and other claudins are higher, this may resemble a more epithelial like phenotype. However, iPS-EC1 expresses other endothelial specific mRNAs, such as the EC specific adhesion molecule ESAM [46] and several brain endothelial cell specific transporters. Hence, iPS-EC1 may have a somewhat mixed endothelial and epithelial phenotype. Contrary to iPS-EC2 and hCMEC/D3, iPS-EC1 shows expression of occludin detectable with immunocytochemistry. Interestingly, occludin levels were reported to be higher in EC in neural tissue than in other EC [47]. These differences in junction associated proteins and mRNA expression may provide clues to why EC derived using different approaches display large differences in TEER and NaF permeability, further discussed below.

Table 3. GO-CC terms enriched in iPS-EC1 after coculture

Name	ID
integrin complex	GO:0008305
cell junction	GO:0030054
extracellular matrix component	GO:0044420
protein complex involved in cell adhesion	GO:0098636
proteinaceous extracellular matrix	GO:0005578
anchored component of membrane	GO:0031225
basement membrane	GO:0005604
cation channel complex	GO:0034703
collagen trimer	GO:0005581
endomembrane system	GO:0012505
intrinsic component of membrane	GO:0031224
membrane microdomain	GO:0098857
membrane raft	GO:0045121
plasma membrane	GO:0005886
plasma membrane bounded cell projection	GO:0120025
potassium channel complex	GO:0034705
receptor complex	GO:0043235
side of membrane	GO:0098552
transporter complex	GO:1990351
voltage-gated potassium channel complex	GO:0008076

Enrichment determined using multiple test correction and adjusted p value <.05.

Coculture with astrocytes, pericytes, and neurons had prominent effects on the paracellular tightness of the EC as measured by TEER and NaF permeability. Both iPS-EC1 and iPS-EC2 showed a significant increase in TEER after the coculture. For iPS-EC1 reduced NaF permeability after coculture was observed. Moreover, iPS-EC1 showed increased mRNA expression and functional efflux by P-gp and BCRP in coculture. The mRNA levels of the investigated transporters P-gp and Glut-1 were similar in iPS-EC1 and iPS-EC2, while BCRP mRNA levels were higher in iPS-EC1. The BCRP activity was dependent on coculture while the P-gp activity was not, showing that iPS-EC1 in coculture have improved restriction of both passive and BBB specific permeability. Interestingly, both iPS-EC1 and iPS-EC2 have lower mRNA levels of caveolin1 in coculture compared to monoculture. Caveolin1 is the main component of caveolae, which are endocytic vesicles providing a route of entry into the brain through the EC. Caveolin1 is downregulated in mature human brain EC [48] and the downregulation of caveolin1 have been suggested as a biomarker of barrier maturation [49].

Other iPSC-derived BBB models, that use Protocol 1 to derive EC, have reported increased TEER but no expression changes in the investigated markers and transporters after coculture [27, 28]. However, one of the studies reported a significant decrease in discontinuous junctions [27]. Other iPSC-derived BBB models have reported an increase in permeability of rhodamine 123 of 40%–50% after treatment with P-gp inhibitors [26, 27], which is slightly higher than the 28% observed in our model. Similar to our results, these studies do not show changes in P-gp efflux activity between monoculture and coculture. In summary, coculture with the iPSC-derived specific NVU cell types improved the TEER for both iPS-EC1 and iPS-EC2, and increased expression of two efflux transporters in iPS-EC1. This indicates that the in vivo-like culture environment created by multiple, readily available cell types improve to the barrier properties of the model. Both iPS-EC1 and iPS-EC2 have lower P-gp than hCMEC suggesting that increased P-gp expression may be one of the improvements needed for iPSC derived models.

To do an initial investigation of how well our iPSC-derived coculture model mimics different forms of barrier transport, we tested the permeability of six drug substances. Substance permeability was most restricted in iPS-EC1 in coculture. Apparent permeability across BBB from in vivo mouse studies was reported to be in the range of 10^{-6} for atenolol, 10^{-5} for verapamil, 10^{-4} for phenytoin, and 10^{-3} for propranolol [50]. Our model shows similar permeability to this in vivo model for the low permeability substances; atenolol and verapamil, and lower permeability for the high passive permeability substances; phenytoin and propranolol. Human data for these substances are not available. Importantly, iPS-EC1 can distinguish between CNS-permeable and non-CNS-permeable substances, whereas iPS-EC2 cannot. Future permeability assessment should focus on substances with available data from human in vivo studies to enable further validation the model.

In drug development, it is desirable that BBB models can distinguish which new drug candidates are substrates for efflux transporters. In this study, we focused on BCRP and P-gp as efflux by these transporters is critically limiting the BBB-penetrating capacity of many drug substances [51]. iPS-EC1 has efflux activity for P-gp and BCRP substrates. iPS-EC2 cells express some P-gp and BCRP mRNA but do not efflux the substrates for these transporters. It is possible that efflux transporters are present and active, although their activities are not measurable due to the low tightness and paracellular leakage in iPS-EC2. To our knowledge, there is no previously published data available on efflux ratios of the tested compounds in iPSC-derived EC. The efflux ratio of human primary brain EC has been reported to be 1.4 for verapamil [9], which is similar to efflux ratio for iPS-EC1 in monoculture. In conclusion, substances that are affected by efflux are more clearly distinguishable using iPSC-EC1.

The mechanisms behind BBB formation are poorly understood and to gain more insight into these processes, we investigated transcriptional changes in the iPSC-derived EC in coculture. A larger number of genes were affected by the coculture for iPS-EC1 as compared to iPS-EC2. Together with the larger changes in tightness seen in iPS-EC1, this suggests that cells derived with iPS-EC1 are more susceptible to cues from surrounding cells than iPS-EC2. By investigating the expression of junction-associated proteins and transporters, we show important differences between iPS-EC1 and iPS-EC2. iPS-EC2 have high expression of CLDN5, ICAM1, ICAM2, PECAM1 (CD31), CDH5 (VE-cadherin), JAM3, and ESAM1, while iPS-EC1 have high expression of CLDN4, CLDN6, and CLDN7. If the differences are present also at protein level, it suggests the possibility to have tight cell–cell adhesion without high expression of many common EC markers. Similarly, claudin 1, 3, 4 have been found to be expressed at higher levels than claudin 5 in ECs derived with protocol 1 [28]. Both VE-cadherin and CD31 have shown to be required for endothelial tube formation in vitro [52], but it is unclear how important they are for cell–cell adhesion in monolayers. iPS-EC1 and iPS-EC2 express different claudin mRNAs and have substantially different TEER. These results implicate the importance of several members of the claudin family for tight junction formation. Other reports have also discussed this matter, for example, CLDN5 knockout mice retain BBB structure and permeability restriction of larger molecules through tight junction formation by other claudins [53]. Our data support previous reports that expression levels of OCLN, CLDN3, CLDN4, CLDN5, CDH5, and TJP1 are not increased after coculture [27, 28]. Interestingly, TJP3 increased for both protocols while CLDN8, and CLDN19 only increased for the iPS-EC1 and CLDN6 increased only for the iPS-EC2. CLDN6 is already highly expressed in iPS-EC1 in both monoculture and coculture. Moreover, expression of CLDN19 and CLDN8

in epithelial cells has previously been described to increase paracellular tightness [54, 55]. Notably, both CLDN8 and CLDN19 have low expression in iPS-EC2, which show higher permeability. We speculate that the junction-associated genes with a significant increase between monoculture and coculture, are contributing to the increase in tightness seen for both protocols in the coculture condition.

The transporter gene SLC6A15 increased significantly in expression between monoculture and coculture for both iPS-EC1 and iPS-EC2. The iPS-EC1 also showed increased expression of ABCB1 and SLC6A13 in coculture compared to monoculture. ABCB1 (P-gp) are among the most abundant transporters found in human brain microvessels [56], SLC6A13 and SLC6A15 are involved in the transport of neurotransmitters across the BBB [57]. The increased expression of these genes suggests that the coculture is affecting the maturity of the EC through increased expression of specific BBB transporters.

GO terms and pathways associated with the genes that are affected by the coculture represent many processes important for the formation of tight cell layers such as cell adhesion, cell junctions, and extracellular matrix. Providing further evidence that coculture is aiding maturation of the EC toward a BBB phenotype. The WNT signaling pathway, the TNF signaling pathway, and the PI3K-Akt signaling pathway were identified as changing in coculture and several mechanisms controlled by these pathways may be important for the BBB formation. TNF signaling impacts the expression of junction-associated proteins in a BBB cell model [24]. In addition, the activity in PI3K-Akt pathway has recently shown to be important for BBB integrity in both mouse and rat [58, 59], and the WNT signaling pathway has previously been indicated in governing BBB formation [17, 24]. In our studies, the expression of BCRP and P-gp were upregulated in coculture. Interestingly, these results correspond well with previous reports that BCRP levels are influenced by the PI3K-Akt and the WNT signaling pathways and that P-gp level are influenced by the TNF and the PI3K-Akt pathways [60]. In other BBB models, coculturing cell types have been suggested to affect EC maturation through the Notch and the Sonic hedgehog pathways [23]. Notably, our analysis did not show significantly changed activity in these pathways after coculture. We hypothesize that coculturing of iPSC-derived cell types may affect EC tightness and maturation through the WNT, PI3K-Akt, and TNF signaling pathways.

CONCLUSION

Our results show that an iPSC-derived BBB model with high tightness, efflux activity, and ability to discriminate between CNS permeable and non-permeable substances can be produced with iPS-EC1. Coculture is affecting the maturity of the EC both

in terms of gene expression and important functionality. The information gained from investigation of the whole genome expression changes that occur in iPSC-derived EC upon coculture will be instrumental in designing novel improvement strategies for in vitro BBB models.

AUTHOR CONTRIBUTIONS

L.D.: conception and design of experiments, collection and assembly of data, data analysis and/or interpretation, manuscript writing, final approval of manuscript; P.D.: data analysis and/or interpretation, manuscript writing, final approval of manuscript; J.S.: data analysis and/or interpretation, final approval of manuscript; M.C.: collection and assembly of data, final approval of manuscript; D.V.: collection and assembly of data, final approval of manuscript; A.F.: data analysis and/or interpretation, final approval of manuscript; A.H.: data analysis and/or interpretation, final approval of manuscript; G.B.: conception and design of experiments, final approval of manuscript; H.Z.: conception and design of experiments, data analysis and interpretation, manuscript writing, final approval of manuscript; R.H.: conception and designed of experiments, data analysis and interpretation, manuscript writing, final approval of manuscript; J.S.: conception and design of experiments, data analysis and interpretation, manuscript writing, final approval of manuscript.

DISCLOSURE OF POTENTIAL CONFLICTS OF INTEREST

The authors indicated no potential conflicts of interest.

REFERENCES

1 Abbott NJ, Patabendige AA, Dolman DE et al. Structure and function of the blood-brain barrier. Neurobiol Dis 2010;37:13–25.
2 Banerjee S, Bhat MA. Neuron-glial interactions in blood-brain barrier formation. Annu Rev Neurosci 2007;30:235–258.

3 Obermeier B, Daneman R, Ransohoff RM. Development, maintenance and disruption of the blood-brain barrier. Nat Med 2013;19: 1584–1596. Review.
4 Neuhaus W, Noe CR. Transport at the blood–brain barrier. *Transporters as Drug Carriers*. Weinheim, Germany: Wiley-VCH Verlag GmbH & Co. KGaA, 2010:263–298.

5 Vandenhaute E, Dehouck L, Boucau MC et al. Modelling the neurovascular unit and the blood-brain barrier with the unique function of pericytes. Curr Neurovasc Res 2011;8: 258–269.
6 Toyoda K, Tanaka K, Nakagawa S et al. Initial contact of glioblastoma cells with existing normal brain endothelial cells strengthen the

barrier function via fibroblast growth factor 2 secretion: a new in vitro blood-brain barrier model. Cell Mol Neurobiol 2013;33:489–501.

7   Xue Q, Liu Y, Qi H et al. A novel brain neurovascular unit model with neurons, astrocytes and microvascular endothelial cells of rat. Int J Biol Sci 2013;9:174–189.

8   Liu WY, Wang ZB, Wang Y et al. Increasing the permeability of the blood-brain barrier in three different models in vivo. CNS Neurosci Ther 2015;21:568–574.

9   Garberg P, Ball M, Borg N et al. In vitro models for the blood-brain barrier. Toxicol In Vitro 2005;19:299–334.

10   Narayanan R, Gunturi SB. In silico ADME modelling: prediction models for blood-brain barrier permeation using a systematic variable selection method. Bioorg Med Chem 2005;13:3017–3028.

11   Cecchelli R, Berezowski V, Lundquist S et al. Modelling of the blood-brain barrier in drug discovery and development. Nat Rev Drug Discov 2007;6:650–661.

12   Patabendige A, Abbott NJ. Primary porcine brain microvessel endothelial cell isolation and culture. Curr Protoc Neurosci 2014;69:1–17.

13   Warren MS, Zerangue N, Woodford K et al. Comparative gene expression profiles of ABC transporters in brain microvessel endothelial cells and brain in five species including human. Pharmacol Res 2009;59:404–413.

14   Deo AK, Theil FP, Nicolas JM. Confounding parameters in preclinical assessment of blood-brain barrier permeation: an overview with emphasis on species differences and effect of disease states. Mol Pharm 2013;10:1581–1595.

15   Syvanen S, Lindhe O, Palner M et al. Species differences in blood-brain barrier transport of three positron emission tomography radioligands with emphasis on P-glycoprotein transport. Drug Metab Dispos 2009;37:635–643.

16   Eigenmann DE, Xue G, Kim KS et al. Comparative study of four immortalized human brain capillary endothelial cell lines, hCMEC/D3, hBMEC, TY10, and BB19, and optimization of culture conditions, for an in vitro blood-brain barrier model for drug permeability studies. Fluids Barriers CNS 2013;10:33.

17   Lim RG, Quan C, Reyes-Ortiz AM et al. Huntington's disease iPSC-derived brain microvascular endothelial cells reveal WNT-mediated angiogenic and blood-brain barrier deficits. Cell Rep 2017;19:1365–1377.

18   Stewart PA, Wiley MJ. Developing nervous tissue induces formation of blood-brain barrier characteristics in invading endothelial cells: A study using quail-chick transplantation chimeras. Dev Biol 1981;84:183–192.

19   Urich E, Lazic SE, Molnos J et al. Transcriptional profiling of human brain endothelial cells reveals key properties crucial for predictive in vitro blood-brain barrier models. PLoS One 2012;7:e38149.

20   Hayashi Y, Nomura M, Yamagishi S et al. Induction of various blood-brain barrier properties in non-neural endothelial cells by close apposition to co-cultured astrocytes. GLIA 1997;19:13–26.

21   Sobue K, Yamamoto N, Yoneda K, et al. Induction of blood-brain barrier properties in immortalized bovine brain endothelial cells by astrocytic factors. Neurosci Res 1999; 35: 155–164. 2000/01/05.

22   Lippmann ES, Azarin SM, Kay JE et al. Derivation of blood-brain barrier endothelial cells from human pluripotent stem cells. Nat Biotechnol 2012;30:783–791.

23   Alvarez JI, Dodelet-Devillers A, Kebir H et al. The hedgehog pathway promotes blood-brain barrier integrity and CNS immune quiescence. Science 2011;334:1727–1731.

24   Cecchelli R, Aday S, Sevin E et al. A stable and reproducible human blood-brain barrier model derived from hematopoietic stem cells. PLoS One 2014;9:e99733.

25   Patel R, Page S, Al-Ahmad AJ. Isogenic blood-brain barrier models based on patient-derived stem cells display inter-individual differences in cell maturation and functionality. J Neurochem 2017;142:74–88.

26   Hollmann EK, Bailey AK, Potharazu AV et al. Accelerated differentiation of human induced pluripotent stem cells to blood-brain barrier endothelial cells. Fluids Barriers CNS 2017;14:9.

27   Canfield SG, Stebbins MJ, Morales BS et al. An isogenic blood-brain barrier model comprising brain endothelial cells, astrocytes, and neurons derived from human induced pluripotent stem cells. J Neurochem 2016; 140:874–888.

28   Appelt-Menzel A, Cubukova A, Gunther K et al. Establishment of a human blood-brain barrier co-culture model mimicking the neurovascular unit using induced pluri- and multipotent stem cells. Stem Cell Reports 2017;8:894–906.

29   Sjogren A-KM, Liljevald M, Glinghammar B et al. Critical differences in toxicity mechanisms in induced pluripotent stem cell-derived hepatocytes, hepatic cell lines and primary hepatocytes. Arch Toxicol 2014;88:1427–1437.

30   Wilson HK, Canfield SG, Hjortness MK et al. Exploring the effects of cell seeding density on the differentiation of human pluripotent stem cells to brain microvascular endothelial cells. Fluids Barriers CNS 2015;12:13.

31   Orlova VV, van den Hil FE, Petrus-Reurer S et al. Generation, expansion and functional analysis of endothelial cells and pericytes derived from human pluripotent stem cells. Nat Protoc 2014;9:1514–1531.

32   Hubatsch I, Ragnarsson EGE, Artursson P. Determination of drug permeability and prediction of drug absorption in Caco-2 monolayers. Nat Protoc 2007;2:2111–2119.

33   Livak KJ, Schmittgen TD. Analysis of relative gene expression data using real-time quantitative PCR and the 2(−Delta-Delta C(T)) Method. Methods 2001;25:402–408.

34   Love MI, Huber W, Anders S. Moderated estimation of fold change and dispersion for RNA-seq data with DESeq2. Genome Biol 2014;15:550.

35   Mi H, Muruganujan A, Casagrande JT et al. Large-scale gene function analysis with the PANTHER classification system. Nat Protoc 2013;8:1551–1566.

36   Bangsow T, Baumann E, Bangsow C et al. The epithelial membrane protein 1 is a novel tight junction protein of the blood-brain barrier. J Cerebral Blood Flow Metab 2008;28:1249–1260.

37   Bauer H-C, Krizbai IA, Bauer H et al. "You Shall Not Pass"—tight junctions of the blood brain barrier. Front Neurosci 2014;8:392.

38   Begley DJ. ABC transporters and the blood-brain barrier. Curr Pharm Des 2004;10:1295–1312.

39   Geier EG, Chen EC, Webb A et al. Profiling solute carrier transporters in the human blood-brain barrier. Clin Pharmacol Ther 2013;94:636–639.

40   da Huang W, Sherman BT, Lempicki RA. Systematic and integrative analysis of large gene lists using DAVID bioinformatics resources. Nat Protoc 2009;4:44–57.

41   Kanehisa M, Goto S. KEGG: kyoto encyclopedia of genes and genomes. Nucleic Acids Res 2000;28:27–30.

42   Minami H, Tashiro K, Okada A et al. Generation of brain microvascular endothelial-like cells from human induced pluripotent stem cells by co-culture with C6 glioma cells. PLoS One 2015;10:e0128890.

43   Lampugnani MG, Resnati M, Raiteri M et al. A novel endothelial-specific membrane protein is a marker of cell-cell contacts. J Cell Biol 1992;118:1511–1522.

44   Morita K, Sasaki H, Furuse M et al. Endothelial claudin: Claudin-5/Tmvcf constitutes tight junction strands in endothelial cells. J Cell Biol 1999;147:185–194.

45   Ding L, Lu Z, Foreman O et al. Inflammation and disruption of the mucosal architecture in claudin-7-deficient mice. Gastroenterology 2012;142:305–315.

46   Nasdala I, Wolburg-Buchholz K, Wolburg H et al. A transmembrane tight junction protein selectively expressed on endothelial cells and platelets. J Biol Chem 2002;277:16294–16303.

47   Hirase T, Staddon JM, Saitou M, et al. Occludin as a possible determinant of tight junction permeability in endothelial cells. J Cell Sci 1997; 110 (Pt 14): 1603–1613.

48   Zhao Z, Nelson AR, Betsholtz C et al. Establishment and dysfunction of the blood-brain barrier. Cell 2015;163:1064–1078.

49   Ribecco-Lutkiewicz M, Sodja C, Haukenfrers J et al. A novel human induced pluripotent stem cell blood-brain barrier model: Applicability to study antibody-triggered receptor-mediated transcytosis. Sci Rep 2018;8:1873.

50   Nakagawa S, Deli MA, Kawaguchi H et al. A new blood-brain barrier model using primary rat brain endothelial cells, pericytes and astrocytes. Neurochem Int 2009;54:253–263.

51   Agarwal S, Hartz AMS, Elmquist WF et al. Breast cancer resistance protein and P-glycoprotein in brain cancer: Two gatekeepers team up. Curr Pharm Des 2011;17:2793–2802.

52   Yang S, Graham J, Kahn JW et al. Functional roles for PECAM-1 (CD31) and VE-cadherin (CD144) in tube assembly and lumen formation in three-dimensional collagen gels. Am J Pathol 1999;155:887–895.

53   Nitta T, Hata M, Gotoh S et al. Size-selective loosening of the blood-brain barrier in claudin-5–deficient mice. J Cell Biol 2003; 161:653–660.

54   Jeansonne B, Lu Q, Goodenough DA et al. Claudin-8 interacts with multi-PDZ domain protein 1 (MUPP1) and reduces paracellular conductance in epithelial cells. Cell Mol Biol (Noisy-le-Grand) 2003;49:13–21.

55 Hou J, Renigunta A, Konrad M et al. Claudin-16 and claudin-19 interact and form a cation-selective tight junction complex. J Clin Invest 2008;118:619–628.

56 Shawahna R, Uchida Y, Decleves X et al. Transcriptomic and quantitative proteomic analysis of transporters and drug metabolizing enzymes in freshly isolated human brain microvessels. Mol Pharm 2011;8:1332–1341.

57 Kristensen AS, Andersen J, Jorgensen TN et al. SLC6 neurotransmitter transporters: structure, function, and regulation. Pharmacol Rev 2011;63:585–640.

58 Wu F, Chen Z, Tang C et al. Acid fibroblast growth factor preserves blood-brain barrier integrity by activating the PI3K-Akt-Rac1 pathway and inhibiting RhoA following traumatic brain injury. Am J Transl Res 2017;9:910–925.

59 Chi OZ, Mellender SJ, Kiss GK et al. Blood-brain barrier disruption was less under isoflurane than pentobarbital anesthesia via a PI3K/Akt pathway in early cerebral ischemia. Brain Res Bull 2017; 131:1–6.

60 Miller DS. Regulation of ABC transporters at the blood-brain barrier. Clin Pharmacol Ther 2015;97:395–403.

See www.StemCells.com for supporting information available online.